

# Evanescent and inertial-like waves in rigidly-rotating odd viscous liquids

E. Kirkinis<sup>†</sup> and M. Olvera de la Cruz

Department of Materials Science & Engineering, Robert R. McCormick School of Engineering and Applied Science, Northwestern University, Evanston IL 60208 USA  
Center for Computation and Theory of Soft Materials, Northwestern University, Evanston IL 60208 USA

(Received xx; revised xx; accepted xx)

Three-dimensional non-rotating odd viscous liquids give rise to Taylor columns and support axisymmetric inertial-like waves [*J. Fluid Mech.*, vol. 973, A30, (2023)]. When an odd viscous liquid is subjected to rigid-body rotation however, there arise in addition a plethora of other phenomena that need to be clarified. In this paper we show that three-dimensional incompressible or two-dimensional compressible odd viscous liquids, rotating rigidly with angular velocity  $\Omega$ , give rise to both oscillatory and evanescent inertial-like waves or a combination thereof (which we call of mixed type), that can be *non-axisymmetric*. By evanescent we mean that along the radial direction, typically when moving away from a solid boundary, the velocity field decreases exponentially. These waves precess in a prograde or retrograde manner with respect to the rotating frame. The oscillatory and evanescent waves resemble, respectively, the body and wall-modes observed in (non-odd) rotating Rayleigh-Bénard convection [*J. Fluid Mech.*, vol. 248, pp. 583-604 (1993)]. We show that the three types of waves (wall, body or mixed) can be classified with respect to pairs of planar wavenumbers  $\kappa$  which are complex, real or a combination, respectively. Experimentally, by observing the precession rate of the patterns, it would be possible to determine the largely unknown values of the odd viscosity coefficients. This formulation recovers as special cases recent studies of equatorial or topological waves in two-dimensional odd viscous liquids which provided examples of the bulk-interface correspondence at frequencies  $\omega < 2\Omega$ . We finally point out that the two and three-dimensional problems are formally equivalent. Their difference then lies in the way data propagate along characteristic rays in three dimensions, which we demonstrate by classifying the resulting Poincaré-Cartan equations.

**Key words:**

---

## 1. Introduction

Odd viscous liquids are dissipationless in the sense that they do not give rise to viscous heating (Landau & Lifshitz 1987). They were systematically studied by Avron (1998), following previous work on the quantum Hall effect (Avron *et al.* 1995). Their constitutive laws however, were already known in the context of polyatomic gases where a detailed experimental and theoretical program was carried-out at Leiden with a *terminus ante quem* in the 1960's (Beenakker & McCourt 1970; Hulsman *et al.* 1970). Recent

<sup>†</sup> Email address for correspondence: kirkinis@northwestern.edu

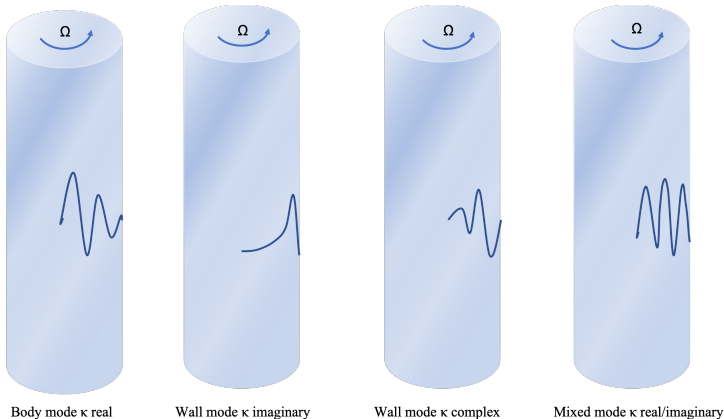


Figure 1: Wall and body modes (or evanescent and oscillatory inertial-like waves, respectively), and mixed mode of the fields (density or pressure  $\sim J_m(\kappa r)$ , where  $J_m$  is the Bessel function of the first kind and  $m$  an integer determining periodicity in the azimuthal direction), for a rigidly-rotating odd viscous liquid with angular velocity  $\Omega$ , in two and three dimensions, satisfying no-slip boundary conditions. Each mode can be classified according to the character of the planar wavenumber  $\kappa$ , cf. table 1. *Body modes*: Prominent in the interior of the cylinder. *Wall modes*: Prominent near the side wall. *Mixed modes*: A combination of the previous two behaviours.

experiments established the existence of odd viscosity in active liquids, which acted to suppress surface undulations in a manner resembling surface tension (Soni *et al.* 2019). In addition to the odd viscosity coefficients cited in the above works, there are others that may appear in materials endowed with discrete symmetries cf. (Rao & Bradlyn 2020; Souslov *et al.* 2020). The review article by Fruchart *et al.* (2023) discusses the above experiments and various physical effects that arise in the presence of odd viscosity.

A previously observed odd viscosity-induced uncommon physical effect, related to the corpus of the present paper is the propagation of inertial-like waves in a three-dimensional odd viscous liquid. This is the case because such a liquid is endowed with an intrinsic mechanism that tends to restore a fluid particle back to its equilibrium position. In addition, a body moving slowly in a quiescent three-dimensional odd viscous liquid will be accompanied by a liquid cylindrical column whose generators circumscribe the body (Kirkinis & Olvera de la Cruz 2023a).

The main result of this paper is the determination of wall and body-like modes in a rigidly-rotating odd viscous liquid with angular velocity  $\Omega$  in a disk or a cylinder of radius  $R$  with no-slip boundary conditions, that resemble their non-odd counterparts in rotating Rayleigh-Bénard convection (Goldstein *et al.* 1993; Knobloch 1994). We identify the wall modes with evanescent waves and the body modes with oscillatory inertial-like waves. Both types can be classified with respect to a single planar wavenumber  $\kappa$ , which is complex or real, respectively cf. Fig. 1. These waves precess in a prograde or retrograde manner with respect to the rotating frame. Wall modes are prominent close to a solid boundary and body modes in the interior of the cylinder (or disk). An odd viscous liquid provides a third case where admissible wavenumbers  $\kappa$  are concurrently real and imaginary, that we call “mixed” in this paper. The classification of the physical behaviours according to the character of  $\kappa$  is displayed in table 1.

Following the theory developed in (Goldstein *et al.* 1993; Knobloch 1994) we obtain

the (exact) fields by satisfying the (no-slip in this paper) boundary conditions. This method provides the admissible curves in the parameter space spanned by the precession frequency  $\omega$  and odd viscosity coefficient  $\nu_o$ , giving rise to the aforementioned behaviour. Thus, it is possible to theoretically determine the largely unknown values of the odd viscosity coefficients by experimentally observing the frequency  $\omega$  of the precessing patterns.

Recent studies on equatorial (Tauber *et al.* 2019) and topological waves (Souslov *et al.* 2019) in two-dimensional odd viscous liquids provided examples of the bulk-interface correspondence by establishing the presence of topological waves at frequencies  $\omega < 2\Omega$ . Our formulation recovers these effects as special cases.

This paper is thus organised as follows. In section 2.1 we formulate the *non-axisymmetric* motion of a two-dimensional compressible rigidly-rotating odd viscous liquid in a disk geometry of radius  $R$  following the arguments developed earlier for (non-odd) rotating Rayleigh-Bénard convection (Goldstein *et al.* 1993; Knobloch 1994) and in (Chandrasekhar 1961). The variable part of the density  $\rho'$ , satisfies a scalar Poincaré-Cartan equation which leads to a relation between the planar wavenumber  $\kappa$ , material parameters and precession frequency  $\omega$  in parameter space. Only one of these wavenumbers  $\kappa$  is however admissible; it can be determined by solving a secular equation obtained by satisfying the (no-slip here) boundary conditions on the side-wall. Thus, the density profiles so obtained, are precessing with frequency  $\omega$  in the rotating frame of the disk and can be exponential or oscillatory in the radial direction. The radially exponential profiles are evanescent waves and resemble the wall modes obtained in (non-odd) rotating Rayleigh-Bénard convection (Goldstein *et al.* 1993; Knobloch 1994), although the wall modes of the latter system are a consequence of thermal forcing and supercritical behaviour of a non-odd system endowed with shear viscosity. The radially exponential profiles can also be understood as equatorial (Tauber *et al.* 2019) and topological waves (Souslov *et al.* 2019) (that is, waves that propagate parallel to a boundary and decay away from it exponentially). Solution of the real and imaginary parts of the secular equation gives parametric curves of admissible  $(\omega, \nu_o)$  values (where  $\nu_o$  is the coefficient of kinematic odd viscosity) leading to the aforementioned exponential/wall mode/evanescent behaviour. Therefore, this formulation can provide the means of determining the largely unknown odd viscosity coefficient by observing the precessing rate of patterns in an experiment. The special case of the axisymmetric  $m = 0$  mode is relegated to the Supplementary Materials addendum that includes a number of illustrative examples associated with this mode.

In section 3 we formulate the non-axisymmetric motion of a *three-dimensional incompressible* rigidly-rotating odd viscous liquid in a cylinder of radius  $R$ . The formulation is nearly identical to the two-dimensional case of section 2.1 with the exception of the presence of an axial velocity component  $v_z(r, \phi, z, t)$ , whose arguments are expressed with respect to cylindrical coordinates, and two (rather than one) odd viscosity coefficients  $\nu_o$  and  $\nu_4$ . A Poincaré-Cartan and a secular equation give rise to the admissible planar real or complex wave-numbers  $\kappa$  leading to precessing body and wall modes, respectively. Since the patterns precess in the rotating frame, again, one could determine the unknown odd viscosity coefficients by experimentally observing their rotation rate. The observation of evanescent waves in rigidly-rotating (non-odd) inviscid or viscous liquids is rather rare with the exception of a recent experimental study (Nosan *et al.* 2021), and references therein. We thus adapt the experimental conditions of Nosan *et al.* (2021) to the case of a three-dimensional odd viscous liquid rotating rigidly with angular velocity  $\Omega$ . We show that fluid particle paths are ellipses lying on  $r - z$  planes and can possibly be employed to determine the unknown values of the odd viscosity coefficients.

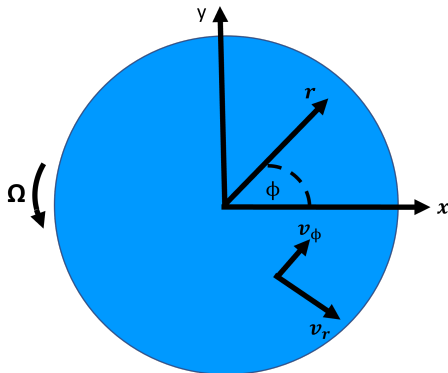


Figure 2: Two-dimensional odd viscous compressible liquid rotating with angular velocity  $\Omega$ . In plane polar coordinates the velocity field is  $\mathbf{v} = v_r \hat{\mathbf{r}} + v_\phi \hat{\boldsymbol{\phi}}$  in the frame rotating with the liquid at constant angular velocity  $\Omega$ .

The two and three-dimensional problems are formally equivalent and the density  $\rho'$  of the former plays the same role as the axial velocity component  $v_z$  in the latter, as discussed in section 3.2. This behaviour is related to the conservation of helicity which is a consequence of the alignment of velocity with vorticity. This tendency of the two fields to alignment, even when *nonlinear* terms of the Navier-Stokes equations are included, is expected from general grounds (Pelz *et al.* 1985). We relegate this discussion to the Supplementary Materials addendum.

The effects described in the main body of this paper are affected by the lower order terms of the governing partial differential equations (the dispersion relation). We show in Appendix B how higher order terms are responsible for the propagation of data in directions explicitly determined by the values taken by the odd viscosity coefficients.

## 2. Evanescent and inertial-like oscillations in a rigidly-rotating compressible two-dimensional odd viscous liquid

### 2.1. Non-axisymmetric waves

A two-dimensional odd viscous liquid obeys the constitutive law (Lapa & Hughes 2014; Ganeshan & Abanov 2017; Banerjee *et al.* 2017)

$$\boldsymbol{\sigma}' = \eta_o \begin{pmatrix} -(\partial_r v_\phi - \frac{1}{r} v_\phi + \frac{1}{r} \partial_\phi v_r) & \partial_r v_r - \frac{1}{r} v_r - \frac{1}{r} \partial_\phi v_\phi \\ \partial_r v_r - \frac{1}{r} v_r - \frac{1}{r} \partial_\phi v_\phi & \partial_r v_\phi - \frac{1}{r} v_\phi + \frac{1}{r} \partial_\phi v_r \end{pmatrix} \quad (2.1)$$

where  $\eta_o$  is termed the odd viscosity coefficient. We here consider a two-dimensional compressible liquid rigidly-rotating with angular velocity  $\Omega$ , endowed with the above constitutive relation and satisfying the continuity equation

$$\partial_t \rho' + \rho \operatorname{div} \mathbf{v} = 0 \quad \text{for} \quad \rho' \ll \rho, \quad (2.2)$$

where  $\rho'$  is the variable part of the density and  $\rho$  a constant background level. In plane polar coordinates  $r, \phi$  (cf. Fig. 2) consider azimuthally-dependent fields of the form

$$[v_r(r), v_\phi(r), \rho'(r)] e^{i(m\phi - \omega t)} \quad (2.3)$$

where  $\omega$  is a real frequency and  $m$  an integer. Employing the constitutive law (2.1), the linearized equations of motion and continuity, in the frame of reference rotating with the

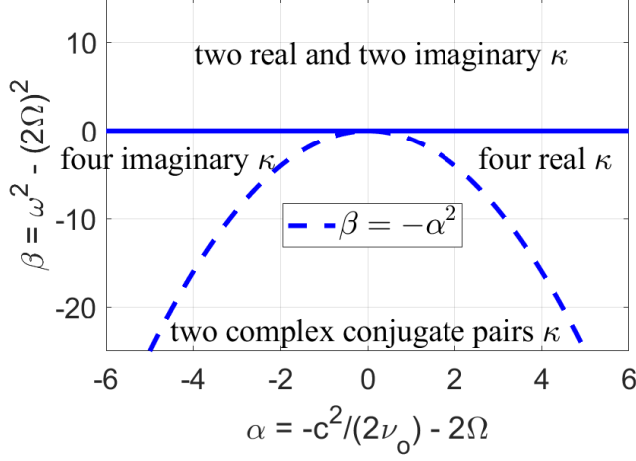


Figure 3: Roots of Eq. (2.12) in the parameter space  $(\alpha, \beta)$  defined in Eq. (2.13) giving rise to the wall and body modes depicted in Fig. 1 according to whether  $\kappa$  is real, imaginary or complex.  $\alpha$  and  $\beta$  have units of frequency and square frequency, respectively.

liquid (Lifshitz & Pitaevskii 1981, §89) become

$$-i\omega v_r = -\frac{c^2}{\rho} \frac{\partial \rho'}{\partial r} + 2\Omega v_\phi - \nu_o \left[ \mathcal{L} v_\phi + \frac{2im}{r^2} v_r \right], \quad (2.4)$$

$$-i\omega v_\phi = -\frac{imc^2}{r} \frac{\rho'}{\rho} - 2\Omega v_r + \nu_o \left[ \mathcal{L} v_r - \frac{2im}{r^2} v_\phi \right], \quad (2.5)$$

$$-i\omega \rho' = -\rho \left[ \frac{1}{r} \frac{\partial}{\partial r} (r v_r) + \frac{im}{r} v_\phi \right], \quad (2.6)$$

where  $c$  is the speed of sound,  $\nu_o = \eta_o/\rho$  and  $\mathcal{L}$  is the linear operator

$$\mathcal{L} = \nabla_2^2 - \frac{1}{r^2}, \quad (2.7)$$

$\nabla_2^2$  is the two-dimensional Laplacian  $\frac{1}{r} \frac{\partial}{\partial r} (r \frac{\partial}{\partial r}) - \frac{m^2}{r^2}$  and we neglected the nonlinear terms assuming small-amplitude motions.

We impose no-slip boundary conditions at  $r = R$

$$v_r(r = R) = v_\phi(r = R) = 0. \quad (2.8)$$

These can be relaxed and replaced by mixed no-slip and force-free boundary conditions as reported in (Souslov *et al.* 2019).

In Appendix C we reduce the momentum and continuity equations into a single equation for the density  $\rho'$

$$\partial_t \left[ (2\Omega - \nu_o \nabla_2^2)^2 - c^2 \nabla_2^2 + \partial_t^2 \right] \rho' = 0. \quad (2.9)$$

Substituting

$$\rho'(r, \phi) = J_m(\kappa r) e^{i(m\phi - \omega t)} \quad (2.10)$$

into (2.9), where  $J_m$  is the Bessel function of first kind, we obtain the relation

$$-\kappa^4 \nu_o^2 - 4\Omega \kappa^2 \nu_o - c^2 \kappa^2 - 4\Omega^2 + \omega^2 = 0, \quad (2.11)$$

---

| $ \alpha^2 + \beta $ |   | $ \alpha $ |   | $ \beta $ |   | Type of root $\kappa$       | Physical effect |
|----------------------|---|------------|---|-----------|---|-----------------------------|-----------------|
| +                    | + | +          | + | +         | + | two real, two imaginary     | Mixed modes     |
| +                    | + | +          | - | +         | + | four real                   | Body modes      |
| +                    | + | -          | - | +         | + | four imaginary              | Wall modes      |
| -                    | - | -          | - | -         | - | two complex conjugate pairs | Wall modes      |

---

Table 1: Types of roots  $\kappa$  displayed in Fig. 3, from Eq. (2.12)  $\nu_o \kappa^2 = \alpha \pm \sqrt{\alpha^2 + \beta}$  according to the sign of the parameters  $\alpha = \frac{\omega^2}{2\Omega_o} - 2\Omega$  and  $\beta = \omega^2 - (2\Omega)^2$  defined in Eq. (2.13). The last column defines the terminology employed in this paper to describe the physical effect

---

satisfied by the (possibly complex) wavenumber  $\kappa = \kappa(c, \Omega, \omega, \nu_o)$ , where all parameters in the round brackets are real. Solving (2.11) for  $\kappa^2$  leads to

$$\nu_o \kappa^2 = \alpha \pm \sqrt{\alpha^2 + \beta}, \quad (2.12)$$

where

$$\alpha = -\frac{c^2}{2\nu_o} - 2\Omega, \quad \beta = \omega^2 - (2\Omega)^2. \quad (2.13)$$

Therefore  $\kappa$  in Eq. (2.12) can be real, imaginary or complex as displayed in, Fig. 3 and Table 1. Each one of these three root types thus corresponds to the three density or pressure behaviours depicted in Fig. 1.

From this point onwards we follow the solution method employed by Goldstein *et al.* (1993) in determining the fields arising in non-odd rapidly-rotating Rayleigh-Bénard convection. From the four values of  $\kappa$  obtained in (2.12), only two give rise to linearly independent solutions. Let  $\kappa_1$  and  $\kappa_2$  denote these  $\kappa$  values. The fields can then be stated as

$$\begin{pmatrix} v_r \\ v_\phi \end{pmatrix} = \sum_{j=1}^2 A_j \gamma_j \begin{pmatrix} \delta_j & 2\Omega \\ -2\Omega & \delta_j \end{pmatrix} \begin{pmatrix} \partial_r \\ \frac{im}{r} \end{pmatrix} J_m(\kappa_j r), \quad \rho' = \sum_{j=1}^2 A_j J_m(\kappa_j r) \quad (2.14)$$

where, the coefficients  $\gamma_j$  and  $\delta_j$  are

$$\gamma_j = \frac{\kappa_j^2 \nu_o + 2\Omega}{2\Omega \kappa_j^2 \rho}, \quad \delta_j = \frac{-2i\omega\Omega}{\nu_o \kappa_j^2 + 2\Omega}, \quad j = 1, 2, \quad (2.15)$$

determined by substituting the solution (2.14) into the continuity equation (2.6) and into the  $z$  component of the vorticity equation, and  $A_j$  are complex constants determined by the boundary conditions. Substituting (2.14) into the boundary conditions (2.8) leads to a homogeneous system for two (complex) equations for the  $A_i$ ,

$$\mathbf{M}(\nu_o, \omega, \Omega, c, \rho, m, R) \begin{pmatrix} A_1 \\ A_2 \end{pmatrix} = 0. \quad (2.16)$$

The complex matrix  $\mathbf{M}$  also depends on  $\kappa_j$  through the dispersion relation. System (2.16) has a solution only when its determinant vanishes, explicitly when

$$\det \mathbf{M} \equiv v_r(\kappa_1 R) v_\phi(\kappa_2 R) - v_r(\kappa_2 R) v_\phi(\kappa_1 R) = 0. \quad (2.17)$$

We thus parameterize  $\kappa_1(\omega, \nu_o)$  and  $\kappa_2(\omega, \nu_o)$ , fix values for  $\Omega, c, \rho, m$  and  $R$ , substitute into the real and imaginary parts of the secular equation (2.17) and solve for  $\omega$  and  $\nu_o$ .

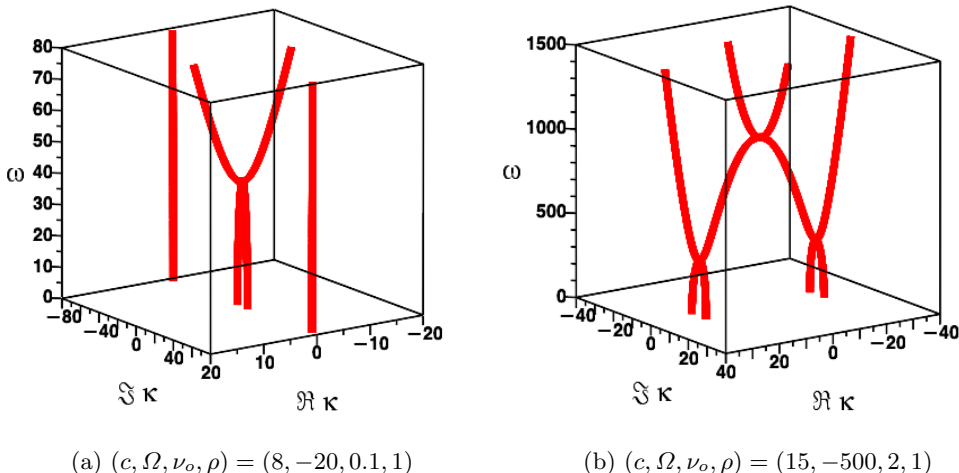


Figure 4: Real frequency  $\omega$  versus the real and imaginary parts of the eigenvalue  $\kappa$  derived as solution of Eq. (2.12). Both panels emphasize the presence of imaginary or complex values of  $\kappa$  that cannot be captured by a plane-wave analysis of the momentum equations. In particular, the domain  $\omega < 2|\Omega|$  is populated by imaginary or complex  $\kappa$ 's that may give rise to wall (evanescent wave) modes (the character of  $\kappa$  is displayed in figure 3). Note that the indicated curves are symmetric with respect to the  $\omega = 0$  plane and continuously extend toward negative  $\omega$  values. The parameters are given in arbitrary units.

## 2.2. Character of the eigenvalue $\kappa$

Recent literature on two-dimensional compressible odd viscous liquids (Tauber *et al.* 2019; Souslov *et al.* 2019) has brought forward examples supporting the bulk-interface correspondence by establishing the presence of waves propagating parallel to a boundary and increasing/decreasing exponentially with distance from it. The starting point for these studies is the dispersion relation  $\omega = \omega(\mathbf{k})$  obtained from (2.11) where  $\mathbf{k}$  is a real wavevector. In this case dispersion curves exist only for  $\omega > 2|\Omega|$ . To obtain the exponential behaviour the wavenumber then is set to be complex and the frequencies studied are those in the “gap”, that is, with  $\omega < 2|\Omega|$ .

We here adopt an opposite outlook, similar to the one followed in the literature of rigidly-rotating liquids. This method emphasizes the derivation of a wavenumber  $\kappa$ , as in Eq. (2.12), that can be complex and is a function of an always real frequency  $\omega$ .

We display in figure 4 the frequency  $\omega$  vs. the real and imaginary parts of  $\kappa$ , drawn from (2.12) which is to be compared with figure 3 and table 1. In panel 4a, when  $\omega < 2|\Omega| = 40$  ( $\beta < 0$ ), the four imaginary roots are clearly visible. When  $\omega > 40 = 2|\Omega|$  ( $\beta > 0$ ), Eq. (2.12) acquires two real and two imaginary  $\kappa$  roots. In panel 4b, when  $\omega < 2|\Omega| = 1000$  ( $\beta < 0$ ), two distinct behaviours are visible. Those that make  $\alpha^2 + \beta$  in (2.12) negative, giving rise to the aforementioned complex roots (located below the parabola of Fig. 3), while those that make  $\alpha^2 + \beta$  positive give rise to four real roots (located outside the parabola of Fig. 3). When  $\beta$  becomes positive ( $\omega > 2|\Omega| = 1000$ ), we obtain two imaginary and two real roots for  $\kappa$ .

The conclusion of this discussion is that values of the frequency  $\omega < 2|\Omega|$  exist when

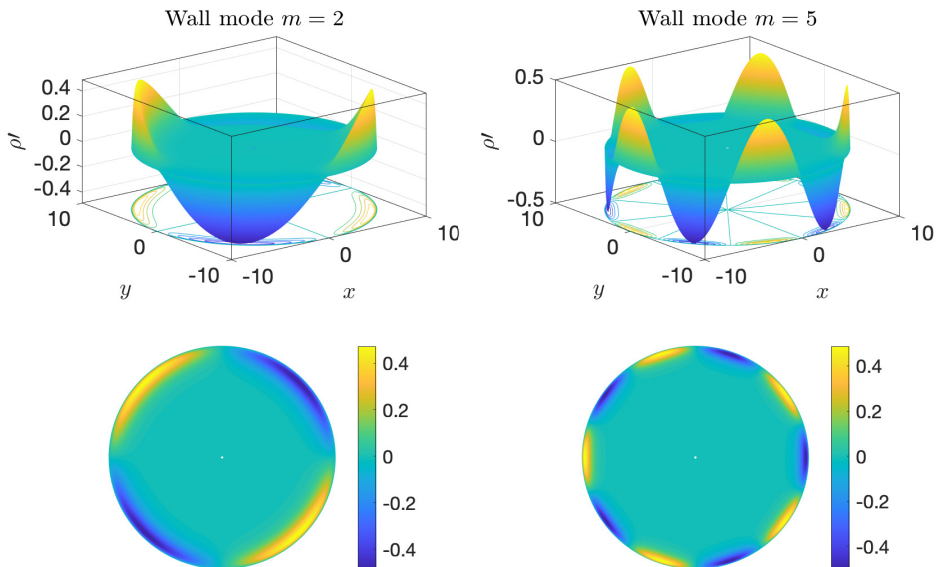


Figure 5: Density profiles and contours for the wall modes arising when the parameter  $\kappa$  lies in the lower left of the diagram 3 (two imaginary pair  $\kappa$ 's) and thus the frequencies lie in the “gap”  $(-2\Omega, 2\Omega)$ . Left column:  $m = 2$  mode, with  $(\omega, \nu_o) = (0.4, 6.4)$  as solution of system (2.17) leading to  $(\kappa_1, \kappa_2) = (-1.95i, -3.2i)$ . Right column:  $m = 5$  mode, with  $(\omega, \nu_o) = (1.5, 2.5)$  as solution of system (2.17) leading to  $(\kappa_1, \kappa_2) = (-2.7i, -5.9i)$ . In both cases  $(c, \Omega, \rho_o, R) = (8, 20, 1, 10)$  and thus both profiles precess in a prograde manner in the frame rotating with the liquid. Note the resemblance of the density profiles with the temperature distribution of rapidly-rotating (non-odd) Rayleigh-Bénard convection in (Goldstein *et al.* 1993, Fig. 6) and of the contour plots with those of Souslov *et al.* (2019, Fig. 3 and S3). Observing experimentally the precession rate of patterns could, in principle, lead to the determination of the odd viscosity coefficient. Parameter and observable units are arbitrary.

the wavenumber  $\kappa$  is imaginary or complex, and this is a natural outcome of the present formulation. Note that both panels in figure 4 symmetrically extend for negative values of the frequency.

### 2.3. Basic observations

From (2.4)-(2.6) we can calculate the vorticity  $\text{curl} \mathbf{v} = \frac{1}{r} \left[ \frac{\partial(rv_\phi)}{\partial r} - \frac{\partial v_r}{\partial \phi} \right] \hat{\mathbf{z}}$  of the two-dimensional odd viscous liquid, which, is found to be proportional to the density  $\rho'$ :

$$\text{curl} \mathbf{v} = (\kappa^2 \nu_o + 2\Omega) \frac{\rho'}{\rho} \hat{\mathbf{z}}. \quad (2.18)$$

This proportionality was also pointed-out in the numerical simulations of Souslov *et al.* (2019, Fig. S2). On account of the equivalence of the two and three-dimensional problem (to be discussed in section 3.2), this proportionality is justified on the basis of conservation of helicity. In addition, it is expected to persist, even when (the neglected here) nonlinear terms are incorporated into the Navier-Stokes equations (Pelz *et al.* 1985). The



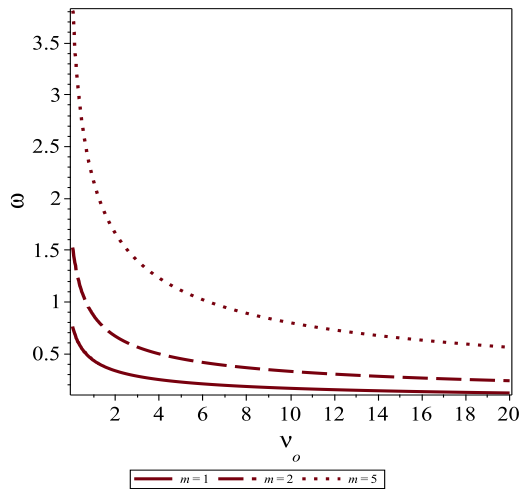


Figure 6: Admissible  $(\nu_o, \omega)$  pairs, as solution of system (2.17), giving rise to the wall modes displayed in Fig. 5, employing the latter figure’s parameter values. Thus, observing experimentally the precession rate of patterns  $\omega$ , it would be possible, in principle, to determine the largely unknown value of the odd viscosity coefficient  $\nu_o$ . Arbitrary units of the parameters were employed.

conservation of helicity follows familiar lines and is thus relegated to the Supplementary Materials addendum.

#### 2.4. Wall and body modes in two-dimensional compressible odd viscous liquids

Goldstein *et al.* (1993); Knobloch (1994), following the experiments of Ecke *et al.* (1992) in rapidly-rotating Rayleigh-Bénard convection (of a non-odd liquid), showed theoretically the existence of two types of non-axisymmetric modes precessing in the rotating system: *Wall modes* which peak near the sidewall and decay in the interior of the cylinder and *body modes* filling the whole cylinder and having their largest amplitudes close to the center rather than the sidewall. Both types are classified in table 1. We proceed by showing that the two-dimensional compressible odd viscous liquid under consideration gives rise to similar wall and body modes which can be understood in the context of our formulation as evanescent and oscillatory inertial-like waves, respectively.

In figure 5 we display the density profiles (first row) for the *wall* modes  $m = 2$  and  $m = 5$  arising by solving the system (2.17) in a disk of radius  $R = 10$  rotating with angular velocity  $\Omega = 20$  and  $\omega > 0$  in both cases (we employ arbitrary units). Thus, the profiles precess with frequency  $\omega$  in a prograde manner in the frame rotating with the disk. Both profiles resemble those of the temperature distribution in (non-odd) rapidly-rotating Rayleigh-Bénard convection as they are displayed in Fig. 6 of Goldstein *et al.* (1993). Note also the resemblance of the contour plots (second row) to the ones of Souslov *et al.* (2019, Fig. 3 and S3).

In figure 6 we display admissible  $(\nu_o, \omega)$  pairs, as solution of system (2.17), giving rise to the *wall* modes displayed in Fig. 5. Thus, all the corresponding  $\kappa$ ’s arising from the displayed parameter pairs are imaginary and will give rise to exponentially decaying velocity fields in the radial direction. Since the modes precess with frequency  $\omega$  in the rotating frame, these modes will also propagate parallel to the circular boundary of the

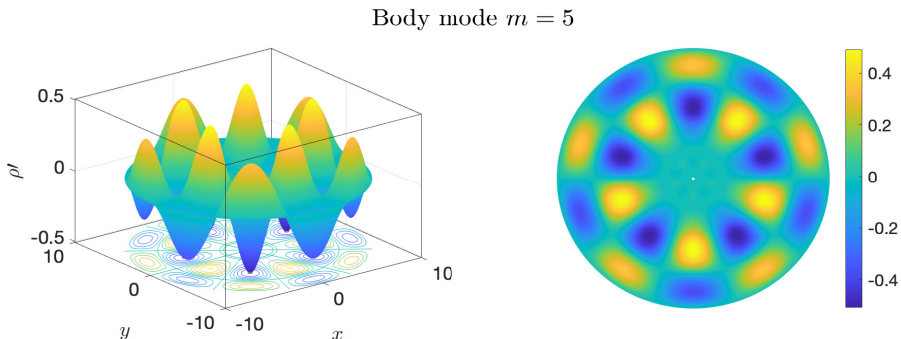


Figure 7: A body mode for  $m = 5$  with  $(\omega, \nu_o) = (34.6, -2.8)$  as solution of system (2.17) leading to  $(\kappa_1, \kappa_2) = (-4.2, 1.7)$ , and same parameters as in Fig. 5. Thus the admissible  $\kappa$ 's are located in the lower right of Fig. 3. The patterns precess in the rotating frame in a prograde manner. Note the resemblance of the density profiles with the temperature distribution of non-odd rapidly-rotating Rayleigh-Bénard convection in (Goldstein *et al.* 1993, Fig. 7). Observing experimentally the precession rate of patterns could, in principle, lead to the determination of the odd viscosity coefficient. Units employed above are arbitrary.

disk. It is thus clear that observing experimentally the precession rate of patterns could, in principle, lead to the determination of the odd viscosity coefficient  $\nu_o$ .

We note that (Favier & Knobloch 2020; Knobloch 2022) commented about the resemblance of wall modes in (non-odd) rapidly-rotating Rayleigh-Bénard convection to odd viscosity-induced topological waves that appear near the boundary of a rotating two-dimensional odd viscous liquid (Souslov *et al.* 2019).

In figure 7 we display the density and contour profile of the *body* mode  $m = 5$  arising by solving the system (2.17) in a disk of radius  $R = 10$  rotating with angular velocity  $\Omega = 20$ . The profile precesses with frequency  $\omega$  in a prograde manner in the frame rotating with the disk. The profile resembles somewhat the temperature distribution in the (non-odd) rapidly-rotating Rayleigh-Bénard convection as they are displayed in Fig. 7 of Goldstein *et al.* (1993).

### 3. Inertial-like waves in a three-dimensional rigidly-rotating incompressible odd viscous liquid

The constitutive law of an odd viscous liquid in three dimensions is of the form

$$\boldsymbol{\sigma}' = \boldsymbol{\sigma}'_o + \boldsymbol{\sigma}'_4, \quad (3.1)$$

where, in cylindrical polar coordinates  $r, \phi, z$ ,

$$\boldsymbol{\sigma}'_o = \eta_o \begin{pmatrix} -(\partial_r v_\phi - \frac{1}{r} v_\phi + \frac{1}{r} \partial_\phi v_r) & \partial_r v_r - \frac{1}{r} v_r - \frac{1}{r} \partial_\phi v_\phi & 0 \\ \partial_r v_r - \frac{1}{r} v_r - \frac{1}{r} \partial_\phi v_\phi & \partial_r v_\phi - \frac{1}{r} v_\phi + \frac{1}{r} \partial_\phi v_r & 0 \\ 0 & 0 & 0 \end{pmatrix}, \quad (3.2)$$

and

$$\boldsymbol{\sigma}'_4 = \eta_4 \begin{pmatrix} 0 & 0 & -(\frac{1}{r} \partial_\phi v_z + \partial_z v_\phi) \\ 0 & 0 & \partial_r v_z + \partial_z v_r \\ -(\frac{1}{r} \partial_\phi v_z + \partial_z v_\phi) & \partial_r v_z + \partial_z v_r & 0 \end{pmatrix} \quad (3.3)$$

|                              |                            |                              |            |
|------------------------------|----------------------------|------------------------------|------------|
| (Lifshitz & Pitaevskii 1981) | (Khain <i>et al.</i> 2022) | (Hulsman <i>et al.</i> 1970) | This paper |
| $\eta_3$                     | $\eta_1^o$                 | $\eta_4$                     | $\eta_o$   |
| $\eta_4$                     | $\eta_2^o$                 | $\eta_5$                     | $\eta_4$   |

Table 2: Conventions of odd viscosity coefficients that have appeared in the literature

where  $\eta_o$  and  $\eta_4$  are the odd viscosity coefficients. Notations employed in the literature to denote the odd viscosity coefficients appear in table 2.

Consider a three-dimensional odd viscous liquid rotating rigidly about the  $\hat{\mathbf{z}}$  axis with angular velocity  $\Omega$  (cf. Fig. 8) and azimuthally-dependent fields

$$[v_r(r), v_\phi(r), v_z(r), p'(r)] e^{i(kz+m\phi-\omega t)} \quad (3.4)$$

in the frame of reference rotating with the liquid, where the frequency  $\omega$  and wave number  $k$  along the axis are both real and  $m$  is an integer. We assume that  $k$  has already been fixed by suitable boundary conditions on the lids of the cylinder. We neglect the nonlinear terms by assuming small-amplitude motions. The Navier-Stokes equations take the form

$$-i\omega v_r - 2\Omega v_\phi = -\frac{1}{\rho} \frac{\partial p'}{\partial r} - \nu_o \left[ \mathcal{L} v_\phi + \frac{2im}{r^2} v_r \right] + \nu_4 \left[ k^2 v_\phi + \frac{mk}{r} v_z \right], \quad (3.5)$$

$$-i\omega v_\phi + 2\Omega v_r = -\frac{im}{r} \frac{p'}{\rho} + \nu_o \left[ \mathcal{L} v_r - \frac{2im}{r^2} v_\phi \right] + \nu_4 \left[ -k^2 v_r + ik \frac{\partial v_z}{\partial r} \right], \quad (3.6)$$

$$-i\omega v_z = -\frac{ik}{\rho} [p' + \eta_4 \zeta], \quad (3.7)$$

where  $\mathcal{L}$  is the linear differential operator (2.7),  $p'$  is the variable part of the pressure in the wave,  $(\nu_o, \nu_4) \equiv (\eta_o, \eta_4)/\rho$  are the coefficients of kinematic odd viscosity,  $\zeta$  is the  $z$  component of the vorticity,  $\zeta = \frac{1}{r} \left[ \frac{\partial}{\partial r} (rv_r) - imv_r \right]$ , and the centrifugal acceleration has been combined into the effective pressure  $p'$ , (Greenspan 1968).

The incompressibility condition becomes

$$\frac{1}{r} \frac{\partial}{\partial r} (rv_r) + \frac{im}{r} v_\phi + ikv_z = 0. \quad (3.8)$$

In Appendix B we derive a single equation for the pressure  $\tilde{p} = p' + \eta_4 \zeta$

$$\left[ \nabla_2^2 + \left( 1 - \frac{(2\Omega - \mathcal{S})^2}{\omega^2} \right) \partial_z^2 \right] \tilde{p} = 0, \quad (3.9)$$

where  $\mathcal{S}$  is the linear operator

$$\mathcal{S} = (\nu_o - \nu_4) \nabla_2^2 + \nu_4 \partial_z^2, \quad (3.10)$$

$\nabla_2^2$  is the two-dimensional (horizontal) Laplacian and we considered perturbations of the pressure  $\sim \exp(-i\omega t)$  with real frequency  $\omega$ . Clearly, when  $\nu_o = \nu_4 = 0$  Eq. (3.9) reduces to the standard Poincaré-Cartan equation (A.1) of non-odd rigidly-rotating liquids.

Substituting

$$\tilde{p}(r, \phi) = J_m(\kappa r) e^{i(kz+m\phi-\omega t)} \quad (3.11)$$

into (3.9), where  $J_m$  is the Bessel function of first kind, leads to a quartic equation for the determination of wavenumber  $\kappa$

$$-\kappa^2 - k^2 \left[ 1 - \frac{(2\Omega + \nu_4 k^2 + (\nu_o - \nu_4) \kappa^2)^2}{\omega^2} \right] = 0. \quad (3.12)$$

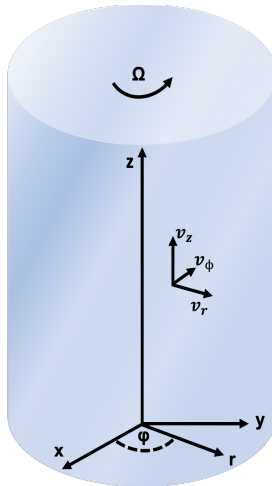


Figure 8: Three-dimensional odd viscous liquid rotating with angular velocity  $\Omega$  about the  $\hat{\mathbf{z}}$  axis. In cylindrical coordinates the velocity field is  $\mathbf{v} = v_r \hat{\mathbf{r}} + v_\phi \hat{\boldsymbol{\phi}} + v_z \hat{\mathbf{z}}$  in the frame of reference rotating with the liquid.

The  $\kappa$  solutions of (3.12) are given by the simple expression

$$\kappa^2 = \frac{\alpha \pm \sqrt{\alpha^2 + \beta}}{2(\nu_o - \nu_4)^2 k^2}, \quad (3.13)$$

with

$$\alpha = \omega^2 + 2k^2 (\nu_4 - \nu_o) (2\Omega + \nu_4 k^2), \quad \beta = 4k^4 (\nu_o - \nu_4)^2 [\omega^2 - (2\Omega + \nu_4 k^2)^2]. \quad (3.14)$$

Thus, the character of  $\kappa$ 's (real, imaginary or complex) is again described by figure 3 and table 1.

From the four values of  $\kappa$  obtained in (3.13), only two give rise to linearly independent solutions. Let  $\kappa_1$  and  $\kappa_2$  denote these  $\kappa$  values. The fields can then be cast as

$$\begin{pmatrix} v_r \\ v_\phi \end{pmatrix} = \sum_{j=1}^2 A_j \gamma_j \begin{pmatrix} \delta_j & 2\Omega \\ -2\Omega & \delta_j \end{pmatrix} \begin{pmatrix} \partial_r \\ \frac{im}{r} \end{pmatrix} J_m(\kappa_j r), \quad v_z = \sum_{j=1}^2 A_j J_m(\kappa_j r), \quad (3.15)$$

the coefficients  $\gamma_j$  and  $\delta_j$  are

$$\gamma_j = \frac{\kappa_j^2 (\nu_o - \nu_4) + \nu_4 k^2 + 2\Omega}{2\Omega \kappa_j^2 \omega}, \quad \delta_j = \frac{-2i\omega\Omega}{\kappa_j^2 (\nu_o - \nu_4) + \nu_4 k^2 + 2\Omega}, \quad j = 1, 2, \quad (3.16)$$

determined by substituting the solution (3.15) into the isochoric constraint (3.8) and into the  $z$  component of the vorticity equation, and  $A_j$  are complex constants to be determined by the boundary conditions.

We impose no-slip boundary conditions at the sidewall of the cylinder  $r = R$

$$v_r(r = R) = v_\phi(r = R) = 0, \quad (3.17)$$

leading to a homogeneous system for two (complex) equations for the  $A_i$ ,

$$\mathbf{M}(\nu_o, \nu_4, \omega, \Omega, k, m, R) \begin{pmatrix} A_1 \\ A_2 \end{pmatrix} = 0. \quad (3.18)$$

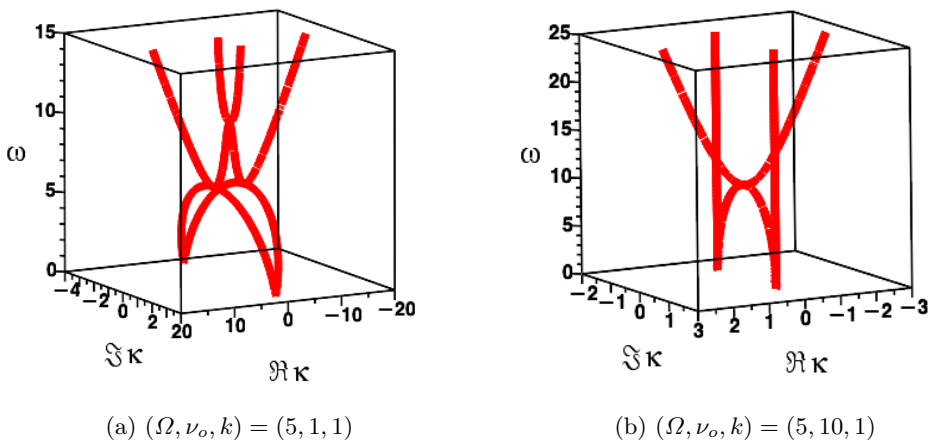


Figure 9: Real frequency  $\omega$  versus the real and imaginary parts of the eigenvalue  $\kappa$  derived as solution of Eq. (3.13). Both panels emphasize the presence of imaginary or complex values of  $\kappa$  that cannot be captured by a plane-wave analysis of the momentum equations. In particular the domain  $\omega < 2\Omega$  is populated by imaginary or complex  $\kappa$ 's that exclusively give rise to wall (evanescent wave) modes. Note that the indicated curves are symmetric with respect to the  $\omega = 0$  plane. Units employed above are arbitrary.

System (3.18) has a solution only when its determinant

$$\det \mathbf{M} \equiv v_r(\kappa_1 R) v_\phi(\kappa_2 R) - v_r(\kappa_2 R) v_\phi(\kappa_1 R) = 0, \quad (3.19)$$

vanishes. We thus parameterize  $\kappa_1(\omega, \nu_o, \nu_4)$  and  $\kappa_2(\omega, \nu_o, \nu_4)$ , fix values for  $\Omega, k, R, m$ , substitute into the real and imaginary parts of (3.19) and solve for  $\omega$  and  $\nu_o$  (see the discussion in section 3.3 on how  $\nu_4$  is chosen).

### 3.1. Character of the $\kappa$ eigenvalues

A non-odd rotating liquid has  $\kappa$  solutions satisfying

$$\kappa = k \sqrt{\frac{4\Omega^2}{\omega^2} - 1} \quad (\text{non-odd rotating liquid})$$

(obtained from the Poincaré-Cartan Eq. (A1)). Thus, when  $\omega < 2\Omega$ ,  $\kappa$  is real and the solutions are oscillatory Bessel functions. When however  $\omega > 2\Omega$ , there are two imaginary  $\kappa$ 's and the fields are modified (exponentially increasing) Bessel functions.

We display in figure 9 the frequency  $\omega$  vs. the real and imaginary parts of  $\kappa$ , drawn from (3.13) which is to be compared with figure 3 and table 1.

In panel 9a we display the bifurcation diagram for the set of values  $(\Omega, \nu_o, k) = (5, 1, 1)$  (arbitrary units). There are two complex conjugate roots up to  $\omega = 6$ , where the radical in (3.13) changes sign. For  $6 < \omega < 10 = 2\Omega$  there are four real roots and beyond this, two imaginary and two real roots. In panel 9b we employ the alternative set of values  $(\Omega, \nu_o, k) = (5, 10, 1)$  (arbitrary units). There are four imaginary  $\kappa$  roots up to  $\omega = 10 = 2\Omega$ . Beyond this there are two imaginary and two real roots.

### 3.2. Formal equivalence of the two- and three-dimensional problems

Setting  $\nu_4 = 0$  in the equations of motion shows that they are equivalent to their two-dimensional counterparts by effecting the correspondence

$$p' = c^2 \rho' \text{ (2D)}, \quad p' = \frac{\rho\omega}{k} v_z \text{ (3D)}. \quad (3.20)$$

The pressure in the two and three-dimensional cases satisfies  $p' = \frac{\rho c^2}{i\omega} \text{div}_2 \mathbf{v}$ , and  $p' = -\frac{\rho\omega}{ik^2} \text{div}_2 \mathbf{v}$ , respectively, where  $\text{div}_2 \mathbf{v} = \frac{1}{r} [\partial_r(rv_r) + imv_\phi]$ . Thus, the two problems are identical inasmuch as the respective dispersion relations are taken into account.

Likewise, the three-dimensional problem with  $\nu_4 \neq 0$  can be recovered from the three-dimensional problem with  $\nu_4 = 0$  by performing the substitution

$$\nu_o \rightarrow \nu_o - \nu_4, \quad \text{and} \quad 2\Omega \rightarrow 2\Omega + \nu_4 k^2. \quad (3.21)$$

Thus, the role of  $\nu_4$  is to renormalize both the angular velocity  $\Omega$  and the odd viscosity coefficient  $\nu_o$ .

The question arises, if the two- and three-dimensional problems are mathematically equivalent, where do they differ? In the Appendix we show that the role of  $\nu_4$  is to alter the direction of propagation of data along characteristics. For instance, when  $\nu_4$  is zero, characteristics are parallel to the  $z$  axis, giving rise to a Taylor column, while when  $\nu_4$  is non-zero they become oblique to the center axis.

### 3.3. Mixed and body modes in a three-dimensional odd viscous liquid

In section 2.4 we illustrated the two-dimensional theory by deriving the density profiles when the wavenumbers  $\kappa$  were all imaginary or all real, thus giving rise to wall and body modes defined in table 1, respectively as these are displayed in figures 5 and 7, respectively. There is a third category however, as this is displayed by the character of wavenumbers  $\kappa$  in the upper part of the diagram 3, where there are concurrent real and imaginary admissible  $\kappa$ 's as solution of equation (2.12). Here we will provide one such example, which is displayed in the left column of Fig. 10.

In three dimensions there are two odd viscosity coefficients and a choice has to be made regarding the solution of secular equation (3.19) (two equations for the determination of  $\omega, \nu_o$  and  $\nu_4$ ). We thus follow (Markovich & Lubensky 2021; Khain *et al.* 2022) who consider the combination

$$\eta_o = 2\eta_4 \quad (3.22)$$

as representing an experimentally-verified case (for polyatomic gases, (Hulsman *et al.* 1970)). See the discussion in (Kirkinis & Olvera de la Cruz 2023a, §8.3) for some consequences of making this choice.

In figure 10 we display the axial velocity profiles (first row) for the *mixed* mode  $m = 2$  and body mode  $m = 5$  arising by solving the system (3.19) in a cylinder of radius  $R = 10$  rotating with angular velocity  $\Omega = 1$ ,  $k = 1$ , employing arbitrary units and enforcing the combination (3.22). Plotting the velocity component  $v_z$  is equivalent to plotting the pressure  $\bar{p} = p' + \eta_4 \zeta$  on account of the connexion (3.7). Note that the non-vanishing  $\nu_4$  has renormalized the cylinder angular velocity  $\Omega$  according to (3.21), making  $\beta = 8.3 > 0$  in (3.14).

As in the two-dimensional case, the outcome of this formulation is to give some means of determining the odd viscosity coefficients by observing experimentally the precession rate of the patterns.

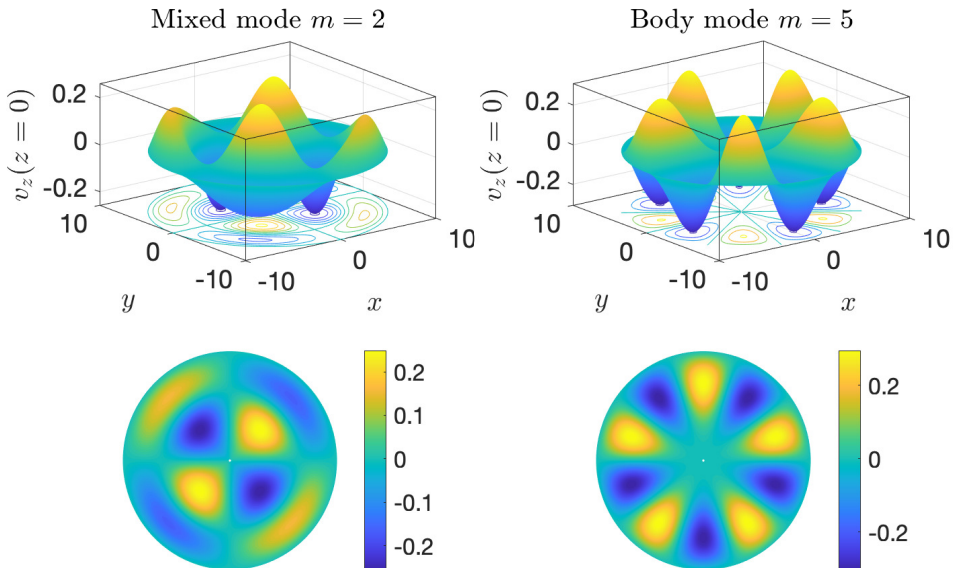


Figure 10: Precessing axial velocity (or pressure) profiles and contours for the modes arising when the parameter  $\kappa$  lies in the upper part (two real two imaginary) and lower right section of the diagram 3 (four real  $\kappa$ 's), respectively. Left column:  $m = 2$  mixed mode, with  $(\omega, \nu_o) = (-0.9, -3.3)$  as solution of system (2.17) leading to  $(\kappa_1, \kappa_2) = (-0.97, -0.5i)$ . Right column:  $m = 5$  body mode, with  $(\omega, \nu_o) = (0.3, -3)$  as solution of system (2.17) leading to  $(\kappa_1, \kappa_2) = (-0.75, 0.3)$ . In both cases  $(k, \Omega, R) = (1, 1, 10)$  in arbitrary units. The odd viscosity coefficients were chosen to satisfy  $\nu_o = 2\nu_4$ , as explained in (3.22). Observing experimentally the precession rate of patterns could, in principle, lead to the determination of the odd viscosity coefficients  $\nu_o$  and  $\nu_4$ . Units employed above are arbitrary.

#### 3.4. Evanescent waves in the experiments of Nosan et al. (2021)

Consider an annular cylinder of inner and outer radii  $R_1$  and  $R_2$ , respectively, where the inner boundary is being radially displaced harmonically with frequency  $\omega$ . The liquid is rotating as a whole with angular velocity  $\Omega$  about the central axis. This then is a system with the geometry employed in the recent experiments of (Nosan *et al.* 2021) which showed that a (non-odd) rigidly-rotating three-dimensional incompressible liquid gives rise to evanescent waves at the cross-over frequency  $\omega \rightarrow 2\Omega$ . Setting  $\omega = 2\Omega$  ( $\beta = 0$  in (3.13)), we obtain two imaginary roots  $\kappa = \pm i\tilde{\kappa}$ , for real  $\tilde{\kappa}$  from (3.13) if  $0 < \Omega < \Omega_o (\equiv \nu_o k^2)$  and the solution reads

$$v_r = AI_1(\tilde{\kappa}r) + BK_1(\tilde{\kappa}r), \quad (3.23)$$

where by  $\tilde{\kappa}$  in this section only we denote the imaginary part of the roots of (3.13). Thus,

$$\tilde{\kappa} = 2\sqrt{\frac{\Omega}{\nu_o} \left(1 - \frac{\Omega}{\Omega_o}\right)}, \quad \Omega_o = \nu_o k^2 > \Omega, \quad (3.24)$$

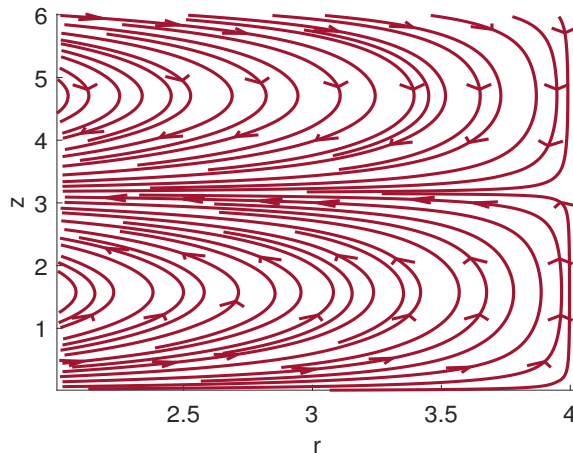


Figure 11: Instantaneous streamlines in the  $r-z$  plane of the velocity field (3.29) - (3.31), representing a forced harmonic wave propagating in the  $z$ -direction according to (3.25). The liquid is confined between the forced inner cylinder at  $r = R_1 = 2 + \text{Re}\eta$  and the immobile external cylinder at  $r = R_2 = 4$  (in arbitrary units).

where, on account of the discussion in the previous paragraph we've set  $\eta_4 \equiv 0$ . Let

$$\eta(z, t) = \hat{\eta} e^{i(kz - \omega t)} \quad (3.25)$$

be the *radial* displacement of the inner boundary at  $r = R_1$  with complex  $\hat{\eta}$  which will excite inertial-like waves of oscillatory or evanescent character. Thus, the radial velocity satisfies

$$v_r(R_1, z, t) = \partial_t \eta = -i\omega \eta, \quad v_r(R_2, z, t) = 0. \quad (3.26)$$

The boundary conditions (3.26) lead to the requirements  $v_r(R_1) = AI_1(\tilde{\kappa}R_1) + BK_1(\tilde{\kappa}R_1) = -i\omega \hat{\eta}$  and  $v_r(R_2) = AI_1(\tilde{\kappa}R_2) + BK_1(\tilde{\kappa}R_2) = 0$  from which we obtain

$$A = -i\omega \hat{\eta} K_1(\tilde{\kappa}R_2) J^{-1}, \quad B = -A \frac{I_1(\tilde{\kappa}R_2)}{K_1(\tilde{\kappa}R_2)}, \quad J = \begin{vmatrix} I_1(\tilde{\kappa}R_1) & I_1(\tilde{\kappa}R_2) \\ K_1(\tilde{\kappa}R_1) & K_1(\tilde{\kappa}R_2) \end{vmatrix}. \quad (3.27)$$

The solution simplifies somewhat if we cast  $A$  in polar form  $A = ae^{i\theta}$  for real  $a, \theta$ . Then,

$$a = \omega |\hat{\eta}| K_1(\tilde{\kappa}R_2) J^{-1}, \quad \theta = -\arctan \frac{\text{Re}\hat{\eta}}{\text{Im}\hat{\eta}}, \quad (3.28)$$

where  $|\hat{\eta}| = \sqrt{(\text{Re}\hat{\eta})^2 + (\text{Im}\hat{\eta})^2}$  and  $\text{Re}\hat{\eta}$  and  $\text{Im}\hat{\eta}$  are the real and imaginary parts of the complex number  $\hat{\eta}$ . We thus obtain,

$$v_r = \omega |\hat{\eta}| J^{-1} [I_1(\tilde{\kappa}r)K_1(\tilde{\kappa}R_2) - I_1(\tilde{\kappa}R_2)K_1(\tilde{\kappa}r)] \cos(kz - \omega t + \theta), \quad (3.29)$$

$$v_\phi = (2\Omega - \nu_o \tilde{\kappa}^2) |\hat{\eta}| J^{-1} [I_1(\tilde{\kappa}r)K_1(\tilde{\kappa}R_2) - I_1(\tilde{\kappa}R_2)K_1(\tilde{\kappa}r)] \sin(kz - \omega t + \theta), \quad (3.30)$$

$$v_z = -\omega |\hat{\eta}| J^{-1} \frac{\tilde{\kappa}}{k} [I_0(\tilde{\kappa}r)K_1(\tilde{\kappa}R_2) + I_1(\tilde{\kappa}R_2)K_0(\tilde{\kappa}r)] \sin(kz - \omega t + \theta). \quad (3.31)$$

Note the positive sign of  $K_0(\tilde{\kappa}r)$  in (3.31) obtained because  $K_n$  satisfies different derivative relations to  $I_n$ . The solution (3.29)-(3.31) for evanescent waves in an odd viscous liquid is formally analogous to the one obtained by Nosan *et al.* (2021). We display the instantaneous resultant streamlines of system (3.29)-(3.31) in an  $r-z$  slice of the cylinder in Fig. 11.



One could attempt to determine the value of odd viscosity with the experimental apparatus of Nosan *et al.* (2021) by measuring the planar velocity  $(v_r, v_\phi)$  at fixed radial locations and different elevations, and averaging the result over a period of oscillation  $2\pi/k$ . These measurements could then be substituted into the expression (determined from equations (3.29) and (3.30))

$$\frac{v_r^2}{[2\Omega(J\tilde{\kappa})^{-1}|\hat{\eta}|\partial_r I(r)]^2} + \frac{v_\phi^2}{[(2\Omega - \nu_o \tilde{\kappa}^2)(J\tilde{\kappa})^{-1}|\hat{\eta}|\partial_r I(r)]^2} = 1, \quad (3.32)$$

which only depends on the radial position of the measurement through the expression  $\partial_r I(r)$ , where

$$I(r) = [I_0(\tilde{\kappa}r)K_1(\tilde{\kappa}R_2) + I_1(\tilde{\kappa}R_2)K_0(\tilde{\kappa}r)]. \quad (3.33)$$

Fixing the  $r$  location, Eq. (3.32) then constitutes one algebraic equation to determine  $\nu_o$ .

The fields (3.29) and (3.31) can also be employed to determine the paths of fluid particles in the wave. Let  $(r_0, z_0)$  and  $(r, z)$  be the equilibrium position and coordinates, respectively, of a moving fluid particle. Let  $dr/dt = v_r$  and  $dz/dt = v_z$  be the velocity of a fluid particle in the  $r - z$  plane and consider small oscillations away from the equilibrium position. Integrating with respect to time gives the trajectories of the fluid particles which are the ellipses

$$\frac{(r - r_0)^2}{[k\partial_r I(r)]^2} + \frac{(z - z_0)^2}{I^2(r)} = [\tilde{\kappa}|\hat{\eta}|J^{-1}]^2. \quad (3.34)$$

Thus, observing the trajectories of suspended particles should, in principle, provide an alternative way of determining the value of the odd viscosity coefficient  $\nu_o$ .

Another related question regards the effect shear viscosity has on the motion of an odd viscous liquid. With respect to the present axisymmetric geometry, the kinematic shear viscosity  $\nu$  enters into the Navier-Stokes equations just by adding the terms  $\nu(\mathcal{L} - k^2)v_r$ ,  $\nu(\mathcal{L} - k^2)v_\phi$  and  $\nu(\mathcal{L} - k^2 + r^{-2})v_z$ , to the right hand side of (3.5), (3.6) and (3.7), respectively, (setting  $m = \nu_4 = 0$ ) everything else remaining the same. Defining the dimensionless frequencies

$$\xi = \frac{\nu k^2}{\omega}, \quad \text{and} \quad \xi_o = \frac{\nu_o k^2}{\omega}, \quad (3.35)$$

and assuming velocity fields of modified Bessel function type  $I_n(k\hat{\kappa}r)$ , leads the dimensionless wavenumber  $\hat{\kappa}$  to satisfy

$$\xi^2 \hat{\kappa}^6 - (\xi_o^2 + 3\xi^2 - 2i\xi) \hat{\kappa}^4 + \left( \frac{4\Omega\xi_o}{\omega} - 1 + 3\xi^2 - 4i\xi \right) \hat{\kappa}^2 - \xi^2 + 2i\xi + 1 - \left( \frac{2\Omega}{\omega} \right)^2 = 0. \quad (3.36)$$

Letting  $\xi_o \equiv 0$  (3.36) recovers the evanescent disturbance wavenumber equation (5.16) of Nosan *et al.* (2021). On the other hand, setting  $\xi = 0$  we recover (3.12). Following the discussion of (Nosan *et al.* 2021), we can study the effects of shear viscosity perturbatively, more specifically, by considering  $\xi$  as a perturbing parameter in Eq. (3.36) and expanding  $\hat{\kappa}$  in powers of  $\xi$ . The wavenumber  $\hat{\kappa}$  correct to first order in  $\xi$  is

$$\hat{\kappa} \sim \frac{\sqrt{2\xi_o - 1}}{\xi_o} + \xi \frac{i(\xi_o - 1)^4}{(2\xi_o - 1)^{\frac{3}{2}} \xi_o^3}. \quad (3.37)$$

Following the program established by Nosan *et al.* (2021), the effect of shear viscosity  $\nu$  on the flow can now be determined by substituting (3.37) into (3.29)-(3.31) and expanding the modified Bessel functions  $I_n(k\hat{\kappa}r)$  and  $K_n(k\hat{\kappa}r)$  with respect to the perturbing parameter  $\xi$ . In the experiments of Nosan *et al.* (2021) (carried-out with a non-odd

viscous liquid), this parameter was equal to 0.008 which led to only modest viscous correction for  $\omega \sim 2\Omega$  (with only one resonant exception). It is clear that these same conclusions are valid in the present case.

#### 4. Conclusion

The main result of this paper is the derivation of precessing wall, body and mixed modes, as these are depicted in Fig. 1 and defined in table 1, in an odd viscous liquid as a consequence of the complex or real character, respectively, of a planar wavenumber  $\kappa$ . The wall modes are evanescent waves and resemble the wall modes obtained in (non-odd) rotating Rayleigh-Bénard convection (Goldstein *et al.* 1993; Knobloch 1994), although the latter are a consequence of thermal forcing in a liquid endowed with shear viscosity. They can also be understood as equatorial (Tauber *et al.* 2019) and topological waves (Souslov *et al.* 2019) (that is, waves that propagate parallel to a boundary and decay away from it exponentially). That these modes should be present in (the dispersive) odd viscous liquid system was also commented by Favier & Knobloch (2020); Knobloch (2022).

The analysis is essentially exact (subject to solving two transcendental equations), and gives rise to a parameter space which could be employed, in principle, to determine the value of the odd viscosity coefficients. In a real system, shear viscosity will be present and it will have to be taken into account. However, by itself, the presence of shear viscosity will always lead an initially forced system to decay in finite time. A meaningful system is one where some form of persistent forcing is always present. For instance in the experiments of Soni *et al.* (2019), which are the only ones where the odd viscosity coefficient has been determined in a liquid, the forcing was provided by a rotating magnetic field. Here, we only discuss some general behaviour of the dispersive system without shear viscosity, with the exception of the (Nosan *et al.* 2021) experiments in section 3.4. Effects of shear viscosity are expected to follow familiar lines of rotating liquids (Chandrasekhar 1961).

In the main body of this article we were concerned with the establishment of fluid flow behaviour that is non-axisymmetric,  $m \neq 0$ . In the Supplementary Materials addendum we provide a detailed discussion of the  $m = 0$  case (axisymmetric) which includes elements of plane polarized waves and the conservation of helicity, following arguments analogous to those of (Kirkinis & Olvera de la Cruz 2023a).

Rotating and stratified Boussinesq flow can be decomposed in parameter regimes depending on the combination of strengths of these two effects (Embid & Majda 1998; Whitehead & Wingate 2014). The typical characteristic of these systems is the existence of a two-dimensional slow manifold towards which energy is being transferred due to fluctuations. Such a two-dimensional manifold is expected to exist in the case of a rigidly-rotating odd viscous liquid although the particle paths of odd viscous liquids are circular while those of internal gravity waves are rectilinear (Maas 2001).

#### Acknowledgments

This research was supported by the US Department of Energy, Office of Science, Basic Energy Sciences under Award No. DE-FG02-08ER46539. The authors are grateful to the anonymous referees for their comments and suggestions that significantly improved the manuscript.

#### Declaration of Interests

The authors report no conflict of interest.

## Appendix A. Poincaré-Cartan equation for a (non-odd) rotating inviscid liquid

For a (non-odd) liquid, rigidly-rotating about the  $z$ -axis with angular velocity  $\Omega$ , the Poincaré-Cartan equation (Greenspan 1968, §2.6), is a second order partial differential equation satisfied by the pressure

$$\left[ \nabla_2^2 + \left( 1 - \frac{4\Omega^2}{\omega^2} \right) \partial_z^2 \right] p' = 0, \quad (\text{A } 1)$$

see also, (Landau & Lifshitz 1987, §14). When  $\omega < 2\Omega$  this equation becomes hyperbolic while, in the opposite case it becomes elliptic, see (Whitham 1974, §12.6). In the hyperbolic case the data propagate on characteristics lying on a cone making an angle  $2\theta$  with the  $z$ -axis, where  $\sin \theta = \omega/(2\Omega)$ . Unsteady motions give rise to inertial waves, that is, plane-polarized waves with  $p' \sim e^{i(\mathbf{k}\cdot\mathbf{r}-\omega t)}$  ( $\mathbf{k} = (k_x, k_y, k_z)$  is the wavenumber whose magnitude is  $k = |\mathbf{k}|$ , and  $\omega$  is the frequency of the inertial wave), and to a dispersion relation  $\omega = 2\Omega k_z/k$ . On the other hand, steady motions ( $\omega \equiv 0$ ) lead to the requirement that  $\partial_z^2 p = 0$ . Characteristics are then straight lines parallel to the  $z$ -axis. Thus, data that emanate from a body moving slowly along the axis of rotation (the  $z$ -axis), propagate in straight lines ahead and behind the obstacle forming Taylor columns (Moore & Saffman 1968; Maxworthy 1970; Bush *et al.* 1994) as long as the group velocity exceeds the speed of the slowly-moving body.

## Appendix B. Poincaré-Cartan equation of three-dimensional odd viscous liquids and its classification

In this section we will derive the Poincaré-Cartan equation for a rigidly-rotating odd viscous liquid, the analogue of (A 1), which is then employed in equations (3.12) and (3.13) to determine the admissible planar wavenumber values. An equivalence between the two and three-dimensional problems was established in section 3.2. Here, we proceed by showing that their difference lies on how data propagate along characteristic rays determined by the values taken over by the odd viscosity coefficients  $\nu_o$  and  $\nu_4$ . This requires the consideration of the higher order terms of the governing PDEs only (the characteristic form), and in doing so we adopt the analysis of Courant & Hilbert (1962, Ch. III, §2.3-2.6).

To this end, the Navier-Stokes equations take the form (when the odd viscous liquid rotates with angular velocity  $\Omega$ ),

$$\frac{\partial u}{\partial t} = -\frac{1}{\rho} \frac{\partial \tilde{p}}{\partial x} + (2\Omega - \mathcal{S})v, \quad \frac{\partial v}{\partial t} = -\frac{1}{\rho} \frac{\partial \tilde{p}}{\partial y} - (2\Omega - \mathcal{S})u, \quad \frac{\partial w}{\partial t} = -\frac{\partial \tilde{p}}{\partial z}, \quad (\text{B } 1)$$

where  $\mathcal{S}$  is the second order differential operator defined in (3.10) and  $\tilde{p} = p' + \eta_4 \zeta$ , with  $\zeta$  being the  $z$ -component of vorticity. In what follows we drop the superposed tilde on the pressure.

To derive the Poincaré-Cartan equation we follow the non-odd, rotating liquid procedure, cf. (Landau & Lifshitz 1987, §14). Differentiate Eq. (B 1) with respect to  $x$ ,  $y$  and  $z$  and add to obtain  $-\nabla^2 p + \rho(2\Omega - \mathcal{S})(\partial_x v - \partial_y u) = 0$  where we employed the incompressibility condition. Differentiating with respect to time and using (B 1) again leads to  $\partial_t \nabla^2 p = -\rho(2\Omega - \mathcal{S})^2 \partial w / \partial z$  by employing the incompressibility condition again. One more differentiation with respect to time and use of the third equation in (B 1) leads

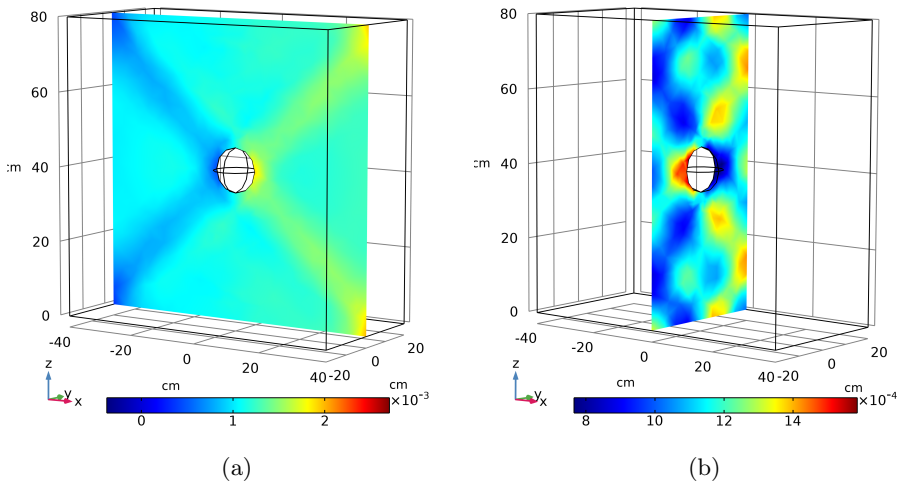


Figure 12: Distribution of pressure (colorbar: dyne/cm<sup>2</sup>) in an odd viscous liquid entering into a rectangular channel from the right, moving slowly with velocity  $U = 0.01$  cm/sec, and meeting a centered solid immobile sphere (of radius 6 cm). Stokes flow with  $\eta_4 = 0.2$  g/(cm sec) and  $\eta_o = 0$  from the constitutive law (3.1), shear viscosity that of water and with no-slip boundary conditions on the channel walls. In both panels data propagate along directions making a 45 degree angle with the horizontal (along the Monge cone  $z = \pm r$  in (B 9)). Since the depth of the box is narrow, the data in panel (b) are reflected on its walls located at  $y = \pm 20$  cm. Numerical simulations were performed with the finite-element package Comsol.

to the desired sixth order equation

$$\left[ \nabla_2^2 + \left( 1 - \frac{(2\Omega - \mathcal{S})^2}{\omega^2} \right) \partial_z^2 \right] p = 0. \quad (\text{B } 2)$$

When  $\nu_o = \nu_4 = 0$  Eq. (B 2) reduces to the standard Poincaré-Cartan equation (A 1). Eq. (B 2) is employed in the main body of this paper to determine the admissible planar wavenumber  $\kappa$  values in equations (3.12) and (3.13).

Eq. (B 2) can be classified according to the scheme employed by Courant & Hilbert (1962, Ch. III, §2.3-2.6) by isolating its principal part  $\partial_z^2 \mathcal{S}^2$ . Thus, the characteristic form is

$$Q(\phi) = \phi_3^2 \mathcal{S}^2(\phi), \quad (\text{B } 3)$$

where

$$\mathcal{S}(\phi) = (\nu_o - \nu_4)(\phi_1^2 + \phi_2^2) + \nu_4 \phi_3^2, \quad (\text{B } 4)$$

$\phi = (\phi_1, \phi_2, \phi_3)$  and the index  $i = 1, 2, 3$  denotes the variables  $x_1 = x, x_2 = y, x_3 = z$  with respect to which the function  $\phi$  is differentiated.

The characteristic form (B 3) is identical to the one obtained from Maxwell's equations (Courant & Hilbert 1962, p. 178) if we identify  $\phi_3$  with  $\tau$  (in Maxwell's case it is exact - there are no lower order terms). In our case there are multiple sheets  $Q_1, Q_2, \dots$  etc., and the characteristic form  $Q$  can be expressed in the form  $Q = Q_1 Q_2 \dots$ , where some of the factors may be identical. Thus, as in (Courant & Hilbert 1962, p. 596) rays should be defined not with reference to  $Q$  but with respect to the irreducible factors  $Q_j$  of  $Q$ . Let

$$Q_1 = \phi_3, \quad \text{and} \quad Q_2 = \mathcal{S}(\phi) \quad (\text{B } 5)$$

be these irreducible factors.

Consider the characteristic surface  $\phi(x, y, z) = c$ , where  $c$  is a constant. The characteristic rays or bicharacteristics are given by

$$\dot{x}_i = \frac{\partial Q}{\partial \phi_i}, \quad i = 1, 2, 3, \quad (\text{B6})$$

where a superposed dot denotes differentiation with respect to some suitable curve parameter  $s$ .

For the first sheet  $Q = Q_1 = \phi_3$ , Eq. (B6) becomes  $dx/ds = dy/ds = 0$  and  $dz/ds = 1$ . Thus, the characteristic curves are

$$\mathbf{C}(s) = (c_1, c_2, c_3) + (0, 0, 1)s, \quad (\text{B7})$$

that is, straight lines in the  $z$  direction away from a fixed point with coordinates  $c_1, c_2, c_3$  and where  $s$  is the parameter of the curve ranging along some suitable interval.

Characteristics are also generated by  $Q_2$  as defined in Eq. (B5). Consider first the special case when  $\nu_4$  vanishes. Then, since  $Q_2 = \phi_1^2 + \phi_2^2$ , we find that characteristics are described by  $\mathbf{C}(s) = (c_1, c_2, c_3)$  since  $Q_2 = 0$  is satisfied only if  $\phi_1 = \phi_2 = 0$ . Thus, when  $\nu_4 = 0$ , the only characteristics associated with the form (B3) are those along the  $z$  direction described in Eq. (B7). This then explains the presence of Taylor columns in a three-dimensional odd viscous liquid which only extend along the  $z$ -direction (Kirkinis & Olvera de la Cruz 2023a).

In the general case where both  $\nu_o$  and  $\nu_4$  are nonzero,  $Q_2 = (\nu_o - \nu_4)(\phi_1^2 + \phi_2^2) + \nu_4\phi_3^2$  from (B5) is substituted into (B6) to give  $dx/ds = (\nu_o - \nu_4)\phi_1$ ,  $dy/ds = (\nu_o - \nu_4)\phi_2$ ,  $dz/ds = \nu_4\phi_3$  (in each case an unimportant factor of 2 has been absorbed into, say,  $s$ ). Take  $z$  to be the time-like variable and form  $\frac{dx}{dz} = \frac{(\nu_o - \nu_4)\phi_1}{\nu_4\phi_3}$  and  $\frac{dy}{dz} = \frac{(\nu_o - \nu_4)\phi_2}{\nu_4\phi_3}$ . From the condition  $Q_2 = 0$  we obtain  $\phi_3^2 = \frac{(\nu_4 - \nu_o)}{\nu_4}(\phi_1^2 + \phi_2^2)$ . This is only possible in the hyperbolic case, requiring that  $\nu_o < \nu_4$  when  $\nu_4 > 0$ . Squaring and adding we obtain

$$\left(\frac{dx}{dz}\right)^2 + \left(\frac{dy}{dz}\right)^2 = \frac{(\nu_4 - \nu_o)}{\nu_4}. \quad (\text{B8})$$

A solution is  $(x - x_0)^2 + (y - y_0)^2 = \frac{(\nu_4 - \nu_o)}{\nu_4}z^2$  where  $x = \alpha_1 z + x_0$  and  $y = \alpha_2 z + y_0$  so,  $\alpha_1^2 + \alpha_2^2 = \frac{(\nu_4 - \nu_o)}{\nu_4}$ . Thus, characteristic curves lie on the local ray cone or Monge cone

$$z = \pm \sqrt{\frac{\nu_4}{\nu_4 - \nu_o}} r \quad (\text{B9})$$

where  $r = \sqrt{(x - x_0)^2 + (y - y_0)^2}$ , see (Courant & Hilbert 1962, p. 601). In Fig. 12 we display two slices of the domain into which liquid enters from the right wall at  $x = 40$  cm. Colorbar denotes the distribution of pressure. In both panels we've set  $\nu_o = 0$  and both panels display the direction of data along characteristics on the local ray cone (B9)  $z = \pm r$ . Figure 12b shows that characteristics are reflected on the lateral channel walls located at  $y = \pm 20$  cm.

In panel (a) of Fig. 13 we display the radial component of the liquid velocity  $\mathbf{v} = v_r \hat{\mathbf{r}} + v_\phi \hat{\boldsymbol{\phi}} + v_z \hat{\mathbf{z}}$  along an  $r$ - $z$  slice of a cylinder (see Fig. 14 for a view of the whole cylinder) filled with odd viscous liquid with  $\eta_4 = 2$  and  $\eta_o = 0.1$  g / (cm sec), and flowing around an immobile sphere (of radius 3.8 cm) located at elevation  $z = 50$ . Liquid enters from the top ( $z = 100$  cm) and exits at the bottom ( $z = 0$ ), with the cylinder speed (the sphere is not allowed to rotate). The white lines are the streamlines of the flow. We thus observe oblique propagation of data from the sphere to the wall and then

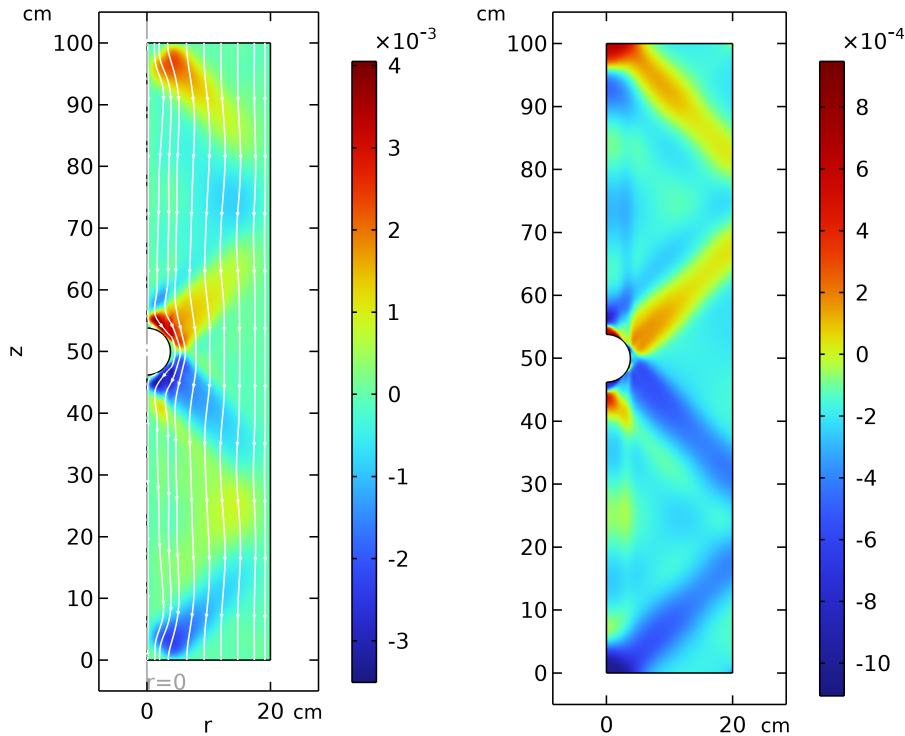
(a) Color-bar: radial velocity  $v_r$  (cm/sec)(b) Colorbar: pressure (dyne/cm<sup>2</sup>)

Figure 13: (a) Colorbar: distribution of radial component of velocity  $v_r$  (cm/sec), (where the liquid velocity is denoted by  $\mathbf{v} = v_r \hat{\mathbf{r}} + v_\phi \hat{\boldsymbol{\phi}} + v_z \hat{\mathbf{z}}$  in cylindrical coordinates) and (b) pressure  $p$  (dyne/cm<sup>2</sup>) in an odd viscous liquid moving slowly and meeting an immobile sphere (of radius 3.8 cm) located at elevation  $z = 50$  cm at the center axis of a cylinder. Here  $\eta_4 = 2$  g/(cm sec),  $\eta_o = 0.1$  g/(cm sec) from constitutive law (3.1), and shear viscosity is that of water. Liquid enters from the top ( $z = 100$  cm) and exits at the bottom ( $z = 0$ ) of the cylinder. The sphere is not allowed to rotate. White lines are liquid streamlines. In all cases data emanating from the sphere propagate along rays that lie on the Monge cone  $z \sim \pm r$  defined in (B 9). A column circumscribing the sphere, whose generators are parallel to the  $z$ -axis is also present. It becomes visible in a plot of the flow structure along the full expanse of the cylinder, see Fig. 14. Numerical simulations were performed with the finite-element package Comsol.

their reflection. In panel (b) of Fig. 13 we display the pressure distribution showing the same pattern of oblique propagation of data. Since there are also characteristics that propagate vertically, associated with the form  $Q_1$  in (B 5), a Taylor-type column also exists, circumscribing the sphere and surrounding the central axis. This becomes visible by displaying the distribution of the axial component of velocity  $v_z$  along the whole cylinder, not just a slice. Thus, in Fig. 14 we see a Taylor column parallel to the anisotropy ( $z$ -axis) circumscribing the sphere, and also oblique characteristics that emanate from the sphere and propagate in a direction making an angle of (nearly) 45 degrees with the horizontal. Parameters employed to produce this figure: Odd viscosity coefficient shear viscosity  $\eta = 0.01$  g/(cm sec), cylinder radius 20 cm, sphere radius 3.8 cm, cylinder height  $H = 100$  cm, liquid density  $\rho = 1$ g/cm<sup>3</sup>, liquid velocity in the  $-\hat{\mathbf{z}}$  direction  $U = 0.01$  cm/sec.

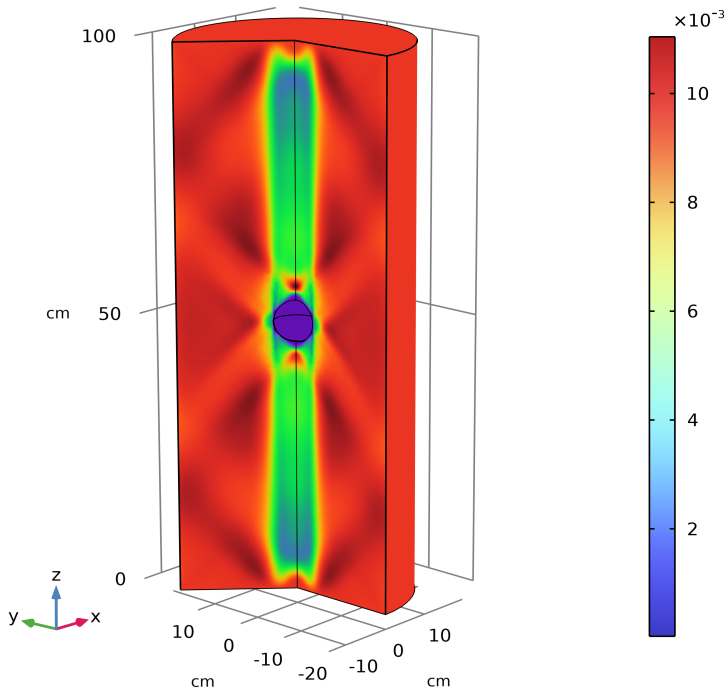


Figure 14: Colorbar: distribution of minus the axial velocity  $v_z$  (cm/sec) (the  $z$ -component of the liquid velocity  $\mathbf{v} = v_r \hat{\mathbf{r}} + v_\phi \hat{\boldsymbol{\phi}} + v_z \hat{\mathbf{z}}$  whose strength is displayed in the colorbar) in an odd viscous liquid moving slowly and meeting an immobile sphere (of radius 3.8 cm) located at elevation  $z = 50$  cm at the center axis of a cylinder (Fig. 13 shows an  $r$ - $z$  slice of this cylinder). Liquid enters from the top ( $z = 100$  cm) and exits at the bottom ( $z = 0$ ). The sphere is not allowed to rotate. The presence of a central Taylor column circumscribing the sphere is visible and it is attributed to the straight-line characteristics (B7) parallel to the anisotropy  $z$ -axis. The presence of rays making (nearly) a 45 degree angle with the horizontal is also visible. They are attributed to the characteristics that lie on the Monge cone (B9).  $\eta_4 = 2$  g/(cm sec),  $\eta_o = 0.1$  g/(cm sec) from constitutive law (3.1), and shear viscosity is that of water, as in Fig. 13. Numerical simulations were performed with the finite-element package Comsol.

Summarizing, the characteristic structures that exist according to the characteristic form (B3) are (assume  $\nu_4 > 0$  for simplicity)

- When  $\nu_o < \nu_4$  then, the operator  $\mathcal{S}$  in (3.10) is hyperbolic and characteristics exist both in the  $z$  direction (because of  $Q_1$  in (B5)) and the oblique direction determined by the ratio of the odd viscosities as in Eq. (B9).
- When  $\nu_o > \nu_4$ , the operator  $\mathcal{S}$  is elliptic and characteristics exist only in the  $z$  direction (because of  $Q_1$  in (B5)).
- When  $\nu_o = \nu_4$ ,  $\mathcal{S}$  is parabolic and characteristics exist only in the  $z$  direction (because of  $Q_1$  in (B5)).

We note that similar conclusions to the above were reached by employing a simpler exposure based on a generalized Taylor-Proudman theorem (Kirkinis & Olvera de la Cruz 2023b).

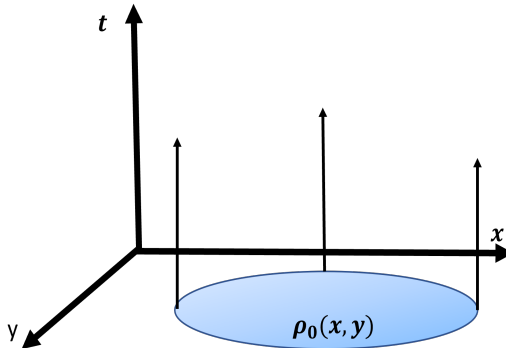


Figure 15: Initial data of density  $\rho_0(x, y)$  in a compressible two-dimensional odd viscous liquid propagate along straight characteristic lines according to Eq. (C 4), forming a temporal Taylor column.

### Appendix C. Poincaré-Cartan equation of a two-dimensional compressible odd viscous liquid

We are not aware of a Poincaré-Cartan equation in two-dimensional compressible flow, so we include below the steps leading to its derivation. This equation is then employed in the main body of this paper to determine the planar wavenumber  $\kappa$  values in Eq. (2.11) and (2.12).

Starting from the Navier-Stokes (by restoring the pressure  $p = \rho' c^2$ ) we obtain the set of equations

$$\partial_t u = -\frac{1}{\rho} \partial_x p + \mathcal{L}v, \quad \partial_t v = -\frac{1}{\rho} \partial_y p - \mathcal{L}u, \quad \partial_t p + \rho c^2 (\partial_x u + \partial_y v) = 0, \quad (\text{C1})$$

where we introduced the linear differential operator  $\mathcal{L} = 2\Omega - \nu_o \nabla^2$ ,  $\rho$  is a constant background density,  $\rho'$  its variable part and  $c$  is the speed of sound. We thus obtain the evolution equations

$$\partial_t (\partial_x v - \partial_y u) = -\mathcal{L}(\partial_x u + \partial_y v), \quad \partial_t (\partial_x u + \partial_y v) = -\frac{1}{\rho} \nabla^2 p + \mathcal{L}(\partial_x v - \partial_y u), \quad (\text{C2})$$

for the vorticity and divergence of the velocity field. Differentiating the pressure equation in (C1) twice and using Eq. (C2) we obtain

$$\partial_t [\mathcal{L}^2 - c^2 \nabla^2 + \partial_t^2] p = 0. \quad (\text{C3})$$

(C3) can be considered as the Poincaré-Cartan equation for a two-dimensional compressible and rigidly-rotating odd viscous liquid. It is clear that when the pressure oscillates as  $e^{-i\omega t}$  one obtains  $\omega [\mathcal{L}^2 - c^2 \nabla^2 - \omega^2] = 0$ , which recovers the dispersion relation (2.12).

The classification of the two-dimensional Poincaré-Cartan equation (C3) can proceed as in the foregoing three-dimensional case (see also (Courant & Hilbert 1962, Ch. III, §2.3-2.6)). We replace the operators  $(\partial_t, \partial_x, \partial_y)$  by time and space-like quantities  $(\tau, \phi_1, \phi_2)$  and form the principal part

$$Q = Q_1 Q_2, \quad \text{where} \quad Q_1 = \tau \quad \text{and} \quad Q_2 = \nu_0 (\phi_1^2 + \phi_2^2)^2. \quad (\text{C4})$$

The situation is the same as in Eq. (B7) with the  $z$  coordinate replaced by time. Initial data propagate along vertical characteristics as displayed in Fig. 15. This situation can also be understood as a *temporal* Taylor column.



## REFERENCES

- AVRON, J.E. 1998 Odd viscosity. *Journal of Statistical Physics* **92** (3-4), 543–557.
- AVRON, J.E., SEILER, R. & ZOGRAF, P.G. 1995 Viscosity of quantum Hall fluids. *Physical Review Letters* **75** (4), 697.
- BANERJEE, D., SOUSLOV, A., ABANOV, A.G. & VITELLI, V. 2017 Odd viscosity in chiral active fluids. *Nature Communications* **8** (1), 1573.
- BEENAKKER, J.J.M. & MCCOURT, F.R. 1970 Magnetic and electric effects on transport properties. *Annual Review of Physical Chemistry* **21** (1), 47–72.
- BUSH, J.W.M., STONE, H.A. & TANZOSH, J.P. 1994 Particle motion in rotating viscous fluids: Historical survey and recent developments. *Current Topics in The Physics of Fluids* **1**, 337–355.
- CHANDRASEKHAR, S. 1961 *Hydrodynamic and hydromagnetic stability*. Oxford University Press.
- COURANT, R. & HILBERT, D. 1962 *Methods of Mathematical Physics. Vol. II: Partial differential equations*. Interscience Publishers (a division of John Wiley & Sons), New York - London.
- ECKE, R.E., ZHONG, F. & KNOBLOCH, E. 1992 Hopf bifurcation with broken reflection symmetry in rotating Rayleigh-Bénard convection. *Europhysics Letters* **19** (3), 177–182.
- EMPID, P.F. & MAJDA, A.J. 1998 Low Froude number limiting dynamics for stably stratified flow with small or finite Rossby numbers. *Geophysical & Astrophysical Fluid Dynamics* **87** (1-2), 1–50.
- FAVIER, B. & KNOBLOCH, E. 2020 Robust wall states in rapidly rotating Rayleigh-Bénard convection. *Journal of Fluid Mechanics* **895**, R1.
- FRUCHART, M., SCHEIBNER, C. & VITELLI, V. 2023 Odd viscosity and odd elasticity. *Annual Review of Condensed Matter Physics* **14**, 471–510.
- GANESHAN, S. & ABANOV, A.G. 2017 Odd viscosity in two-dimensional incompressible fluids. *Physical Review Fluids* **2** (9), 094101.
- GOLDSTEIN, H.F., KNOBLOCH, E., MERCADER, I. & NET, M. 1993 Convection in a rotating cylinder. Part 1 Linear theory for moderate Prandtl numbers. *Journal of Fluid Mechanics* **248**, 583–604.
- GREENSPAN, H.P. 1968 *The theory of rotating fluids*. Cambridge Univ Press.
- HULSMAN, H., VAN WAASDIJK, E.J., BURGMANS, A.L.J., KNAAP, H.F.P. & BEENAKKER, J.J.M. 1970 Transverse momentum transport in polyatomic gases under the influence of a magnetic field. *Physica* **50** (1), 53–76.
- KHAIN, T., SCHEIBNER, C., FRUCHART, M. & VITELLI, V. 2022 Stokes flows in three-dimensional fluids with odd and parity-violating viscosities. *Journal of Fluid Mechanics* **934**, A23.
- KIRKINIS, E. & OLVERA DE LA CRUZ, M. 2023a Taylor columns and inertial-like waves in a three-dimensional odd viscous liquid. *Journal of Fluid Mechanics* **973**, A30.
- KIRKINIS, E. & OLVERA DE LA CRUZ, M. 2023b Taylor halos and Taylor spears in odd viscous liquids. *Physics of Fluids* **35** (10), 101702.
- KNOBLOCH, E. 1994 Bifurcations in rotating systems. In *Lectures on solar and planetary dynamos* (ed. M.R.E. Proctor & A.D. Gilbert), pp. 331–372. Cambridge: Cambridge University Press.
- KNOBLOCH, E. 2022 Geostrophic turbulence and the formation of large scale structure. In *Mathematical and Computational Models of Flows and Waves in Geophysics*, pp. 1–34. Springer.
- LANDAU, L. D. & LIFSHITZ, E. M. 1987 *Fluid Mechanics. Course of Theoretical Physics, Vol. 6*. Pergamon Press Ltd., London-Paris.
- LAPA, M.F. & HUGHES, T.L. 2014 Swimming at low Reynolds number in fluids with odd, or Hall, viscosity. *Physical Review E* **89** (4), 043019.
- LIFSHITZ, E. M. & PITAEVSKII, L. P. 1981 *Course of theoretical physics. Vol. 10: Physical Kinetics*. Pergamon Press.
- MAAS, L.R.M. 2001 Wave focusing and ensuing mean flow due to symmetry breaking in rotating fluids. *Journal of Fluid Mechanics* **437**, 13–28.
- MARKOVICH, T. & LUBENSKY, T.C. 2021 Odd viscosity in active matter: microscopic origin and 3d effects. *Physical Review Letters* **127** (4), 048001.

- MAXWORTHY, T. 1970 The flow created by a sphere moving along the axis of a rotating, slightly-viscous fluid. *Journal of Fluid Mechanics* **40** (3), 453–479.
- MOORE, D.W. & SAFFMAN, P.G. 1968 The rise of a body through a rotating fluid in a container of finite length. *Journal of Fluid Mechanics* **31** (4), 635–642.
- NOSAN, Ž., BURMANN, F., DAVIDSON, P.A. & NOIR, J. 2021 Evanescent inertial waves. *Journal of Fluid Mechanics* **918**, R2.
- PELZ, R.B., YAKHOT, V., ORSZAG, S.A., SHTILMAN, L. & LEVICH, E. 1985 Velocity-vorticity patterns in turbulent flow. *Physical Review Letters* **54** (23), 2505.
- RAO, P. & BRADLYN, B. 2020 Hall viscosity in quantum systems with discrete symmetry: point group and lattice anisotropy. *Physical Review X* **10** (2), 021005.
- SONI, V., BILIGN, E.S., MAGKIRIADOU, S., SACANNA, S., BAROLO, D., SHELLEY, M.J. & IRVINE, W.T.M. 2019 The odd free surface flows of a colloidal chiral fluid. *Nature Physics* **15** (11), 1188–1194.
- SOUSLOV, A., DASBISWAS, K., FRUCHART, M., VAIKUNTANATHAN, S. & VITELLI, V. 2019 Topological waves in fluids with odd viscosity. *Physical Review Letters* **122** (12), 128001.
- SOUSLOV, A., GROMOV, A. & VITELLI, V. 2020 Anisotropic odd viscosity via a time-modulated drive. *Physical Review E* **101** (5), 052606.
- TAUBER, C., DELPLACE, P. & VENAILLE, A. 2019 A bulk-interface correspondence for equatorial waves. *Journal of Fluid Mechanics* **868**, R2.
- WHITEHEAD, J.P. & WINGATE, B.A. 2014 The influence of fast waves and fluctuations on the evolution of the dynamics on the slow manifold. *Journal of Fluid Mechanics* **757**, 155–178.
- WHITHAM, G.B. 1974 *Linear and Nonlinear Waves*. Wiley, NY.